Mother cells control daughter cell proliferation in intestinal organoids to minimize proliferation fluctuations.

Guizela Huelsz-Prince[1], Rutger N.U. Kok[1], Yvonne J. Goos[1], Lotte Bruens[2], Xuan Zheng[1], Saskia I. Ellenbroek[2], Jacco van Rheenen[2], Sander J. Tans[1] , Jeroen S. van Zon[1*]

[1]AMOLF, Science Park 104, 1098 XG, Amsterdam, The Netherlands

[2]Department of Molecular Pathology, Oncode Institute, Netherlands Cancer Institute, 1066 CX Amsterdam, the Netherlands.

[*]corresponding author: Jeroen S. van Zon

Abstract

During renewal of the intestine, cells are continuously generated by proliferation of stem and transit amplifying cells. To ensure homeostasis, proliferation and differentiation must be tightly balanced, with any bias towards proliferation resulting in uncontrolled exponential growth. Yet, the inherently stochastic nature of cells raises the question how such fluctuations are limited. We addressed it using a novel experimental approach. Through time-lapse microscopy, we tracked all individual cells in crypts of growing intestinal organoids for multiple generations, allowing full reconstruction of the underlying lineage dynamics in space and time. We found that proliferative behavior was highly symmetric between sister cells, with both sisters either jointly ceasing or continuing to proliferate. Simulations revealed that such symmetric proliferative behavior minimizes cell number fluctuations, and explained the observed constant numbers of proliferating cells even as crypts increased in size considerably. Proliferative symmetry was preserved for sisters with different distances to Paneth cells, which provide short-range proliferative signals. Hence, proliferative symmetry did not reflect positional symmetry in the crypt, but rather control through the lineage by the mother cell. Clone size distributions obtained in mice confirmed symmetry of proliferation also *in vivo*. Our results indicate a concrete mechanism by which the intestinal epithelium balances proliferation and differentiation with minimal fluctuations, and suggests that it may be more broadly relevant for other tissues.

Significance statement

Tissue maintenance requires constant birth of proliferating cells to offset their loss through terminal differentiation. While any misbalance between birth and loss of proliferating cells could lead to their overgrowth or depletion, the decision to proliferate or not is stochastic, causing fluctuations. How is stable maintenance ensured despite these fluctuations? We study cell proliferation by a novel approach, tracking all cells in crypts of intestinal organoids to fully reconstruct cell lineages. Combined with simulations, our results imply that fluctuations in cell proliferation are minimized by a mechanism that couples strong symmetry in proliferative behavior between sister cells with the partitioning of crypts in compartments of different proliferative potential. This mechanism likely applies to a broader class of stem cell systems.

Introduction

Most adult organs and tissues constantly renew themselves by replacing old and damaged cells, while retaining their structure [1]. Theory indicates that this homeostasis requires a precise balance between proliferating and non-proliferating cells, as even a slight systematic bias towards producing proliferating cells yields uncontrolled exponential cell growth [2-7]. Moreover, the exponential nature of proliferation also readily amplifies fluctuations in the numbers of proliferating cells, which can lead to stochastic cell overgrowth or depletion in absence of additional control mechanisms [8, 9]. How cell proliferation is balanced despite fluctuations has remained challenging to test in direct experiments, given the difficulties of following this process in time.

The mammalian intestine has become an important model system to study the mechanisms of tissue renewal and homeostasis[1, 10]. The proliferating stem cells that sit at the base of intestinal crypts generate rapidly dividing transit-amplifying (TA) cells that in turn replenish the absorptive and secretory cells populating the lining of intestinal villi. Paneth cells positioned at the crypt bottom provide short-range signals that affect the proliferative and undifferentiated state of intestinal stem cells [11-13]. Originally, it was proposed that one or a few stem cells generated all differentiated cells by strictly asymmetric cell divisions [14, 15], thus directly ensuring a constant stem cell pool. Subsequent studies rather suggested that individual cells stochastically and independently cease to divide or not[6, 16, 17]. In this 'population asymmetry' model, in principle one stem cell daughter could remain proliferative by staying adjacent to a Paneth cell, while the other daughter exits the stem cell niche, differentiates, and stops proliferating. However, such asymmetric outcome is no longer guaranteed. Instead, proliferation and differentiation are balanced more indirectly, by averaging these stochastic events across the total stem cell population.

Observations of neutral drift, in which the offspring of a single cell randomly take over the stem cell population of intestinal crypts [6, 16, 17] established the stochastic nature of stem cell proliferation that distinguishes the population asymmetry model from the earlier division asymmetry model. However, approaches used thus far do not follow the underlying cell divisions and lineages in time. Proliferation symmetry between sister cells and its role in homeostasis of the intestinal epithelium have so far only been inferred indirectly, typically by quantifying the clone size distributions at a certain time point. Hence, we also lack insight into the fluctuations of proliferating cells and the mechanisms that control them.

Here, we developed an alternative approach: we employed time-lapse microscopy and single-cell tracking of all cells in crypts of mouse intestinal organoids [18], thus providing complete lineage trees, division dynamics, and cell movement, and combine it with mathematical modelling and intravital imaging of the mouse intestine. Surprisingly, we found that most cell divisions (>90%) were symmetric in proliferative outcome, producing daughter cells that either both continued to proliferate or both ceased proliferating. Proliferation was symmetric even when one daughter neighbored a Paneth cell, the source of proliferative signals in the crypt, while the other did not. Hence, proliferation was not independent between sisters, but rather controlled through the lineage by the mother. Our data and simulations explained not only how this behavior achieves homeostasis, but moreover, that it constitutes a near-optimal strategy to minimize fluctuations in the number of proliferating cells. Consistently, despite their large size increases over multiple generations in crypts of various size, the number of proliferating cells was notably constant in time and exhibited sub-Poissonian fluctuations,

indicating a precise balance between proliferative and non-proliferative sister pairs. Finally, by measuring clone size distributions in mice, we showed that stem cell divisions *in vivo* reproduced the strong symmetry in proliferative behavior between sister cells seen in organoids. As cell proliferation in many tissues follows inherently stochastic 'population asymmetry' mechanisms [3, 16, 19-21], we conjecture that high symmetry in proliferative behavior, controlled through the lineage, may be a more general mechanism to limit proliferation fluctuations.

Results

Single-cell tracking of complete crypts in growing intestinal organoids

To examine the dynamics of individual cells within crypts during growth, we used organoids with a H2B-mCherry nuclear reporter (**Fig. 1A**) and performed confocal 3D time-lapse microscopy for up to 65 hours at a time resolution of 12 minutes. Cell division events were distinguished by the apical displacement of the mother cell nucleus, followed by chromosome condensation and separation, and finally, basal migration of the daughter cell nuclei (**Fig. 1B**), consistent with epithelial divisions[22]. Custom-written software was used to track every cell within organoid crypts by recording their nuclei positions in 3D space and time (**Fig. 1C**) and reconstruct lineage trees containing up to six generations (**Fig. 1F**, **Fig. S1**).

To study the cell lineages along the crypt surface, we 'unwrapped' the crypts: First, we annotated the crypt axes at every time point, then projected every cell position onto the surface of a corresponding cylinder, which we then unfolded (**Fig. 1D,E**). This allowed us to visualize the cellular dynamics in a two-dimensional plane defined by two coordinates: the position along the axis and the angle around the axis. We found that lineages starting close to the crypt bottom typically continued to proliferate and expand in cell number, while those further up in the crypt contained cells that no longer divided during the experiment, consistent with stem cells being located at the crypt bottom and terminal differentiation occurring higher up along the crypt axis (**Fig. 1F**). Lineages were also terminated by the death of cells, as observed by their extrusion into the lumen. This fate occurred more often in some lineages compared to others, and the frequency did not depend strongly on position along the crypt-villus axis. At the crypt bottom we also observed a small number of non-dividing cells, suggestive of terminally differentiated Paneth cells. Indeed, these cells typically exhibited the larger cell size and granules typical of Paneth cells.

Control of cell proliferation in organoid crypts

To systematically study proliferation control, we classified cells as proliferating when they divided during the experiment or non-proliferating when they did not (See **Materials and Methods** for details). When we quantified the total number of cells in the tracked cell lineages for nine crypts, we found a strong (~4-fold) increase in time (**Fig. 2A)**. In contrast, the number of proliferating cells remained approximately constant in time for most crypts (**Fig. 2B)**. Two crypts (crypt 3 and 4 in **Fig. 2**) formed an exception with ~2-fold increase in the number of proliferating cells, an observation that we discuss further below. We then estimated the exponential growth rate α for each crypt, by fitting the dynamics of total cell number and proliferating cell number to a simple model of cell proliferation (**Materials and Methods**). Apart from Crypts 3 and 4, that displayed growth ($\alpha \approx 0.3$), the remaining crypts

showed a low growth rate, $\alpha=0.05\pm0.07$ (**Fig. S2A-C**), indicating that birth of proliferating and non-proliferating cells was balanced on average. We then quantified the magnitude of fluctuations in the number of proliferating cells, D. Calculations of birth-death models of cell proliferation show that, without any control, the standard deviation of the proliferating cell number grows in time without bounds as $\sigma_D \sim \sqrt{Dt}$ [8]. In models without exponential growth, with proliferating cells born at constant rate, fluctuations are reduced: they are constant in time and Poissonian, $\sigma_D \sim \sqrt{D}$ [23]. In models where exponential growth was controlled by homeostatic feedback loops, fluctuations were further reduced to sub-Poissonian: $\sigma_D < \sqrt{D}$ [9]. Using the same measures, we found here that most crypts exhibited sub-Poissonian fluctuations (**Fig. S2D**), implying the presence of a mechanism to limit fluctuations in proliferating cell number. Finally, we quantified the frequency of cell divisions along the crypt axis. Notably, divisions occurred in a region below 60 µm from the crypt base throughout the experiment, even as the crypts grew significantly (**Fig. 2C**), indicating that the size of the proliferative region was constant in time. Moreover, the proliferative region was found to have a similar size in all analyzed crypts (**Fig. 2D**), even though crypts varied both in size, as measured by diameter (30-50 µm, **Fig. S2E**), and number of proliferating cells (**Fig. 2B**). Overall, these results show that crypts by themselves are already capable of a specific form of homeostasis, namely maintaining a stationary number of proliferating cells that occupy a region of the crypt of constant size.

Symmetry of proliferative behavior between sister cells

To examine the origin of the observed balance between the birth of proliferating and non-proliferating cells, we first studied how this balance was maintained between sister cells. First, we examined whether cell proliferation or cell death were correlated between sisters, for all observed sister pairs S_1 and S_2 (**Fig. 3A**). We found that sister pairs showed cell death more rarely than division arrest in at least one of the sisters (16% vs. 54%), indicating that cell death played a minor role in balancing cell proliferation. Moreover, the decision to divide or not was strikingly symmetrical between sisters. In particular, occurrences where on sister divided but the other not were rare (6%) compared to cases where both divided or stopped dividing (78%). This correlation was also apparent by visual inspection of individual lineages, as sisters showed the same division behavior (**Fig. 3B**, top). We also compared lineage dynamics between all cousin pairs C_1 and C_2 (**Fig. 3A**). While we indeed found a significantly increased fraction (12%) of cousin pairs with asymmetrical division outcome, i.e. C_2 dividing and C_1 not, compared to sister pairs (6%), this fraction was still low, indicating that symmetric outcomes also dominated for cousins.

We found that symmetry between sisters did not only impact proliferation arrest, but also cell cycle duration: when a cell exhibited a longer-than-average cell cycle, this was typically mirrored by a similar lengthening of the cell cycle of its sister (**Fig. 3B**, bottom). Indeed, cell cycle duration was strongly correlated between sisters (R=0.8, **Fig. 3C**), even as cell cycle duration showed a broad distribution among tracked cells (**Fig. S3**). In contrast, cell death was not symmetric between sisters, as the fraction of pairs where both cells died (0.03) was smaller than the fraction of pairs where only a single sister died (0.13, **Fig. 3A**).

Symmetry between sisters minimizes fluctuations in a cell proliferation model

In principle, any combination of (a)symmetric divisions would yield a constant number of proliferating cells on average, as long as the birth of proliferating and non-proliferating cells is balanced. We therefore hypothesized that the observed dominance of symmetric divisions might have a function specifically in controlling *fluctuations* in the number of proliferating cells. To test this hypothesis, we used mathematical modelling. Mathematical models of intestinal cell proliferation have been used to explain observed clone size statistics of stem cells [6, 16, 17, 24], but so far not to examine the impact of division (a)symmetry on cell number fluctuations.

We first examined this in context of the canonical stochastic stem cell model[3], that we here refer to as the Uniform model. This model only considers cells as 'proliferating' or 'non-proliferating' (approximating stem and differentiated cells) and tissues that are unbounded in size, while ignoring spatial cell distributions. The parameter ϕ describes the division symmetry, with $\phi=1$ corresponding to purely symmetric divisions and $\phi=0$ to purely asymmetric divisions. The growth rate α describes the proliferation bias, with $\alpha>0$ indicating more proliferating daughters, and $\alpha<0$ more non-proliferating daughters on average. In our simulations, cells either divide symmetrically to produce two proliferating cells with probability $\frac{1}{2}(\phi+\alpha)$ or two non-proliferating cells with probability $\frac{1}{2}(\phi\text{-}\alpha)$, while the probability to divide asymmetrically is $1\text{-}\phi$ (**Fig. 4A**). The number of proliferating cells increases exponentially for $\alpha>0$ or decreases exponentially for $\alpha<0$ while homeostasis requires $\alpha=0$ [2, 3] (**Fig. 4B**).

When varying the division symmetry ϕ while maintaining α=0, we found that fluctuations in the number of proliferating cells D were minimized for ϕ=0 (**Fig. 4B, C**), i.e. every division was asymmetric. In this scenario, the number of proliferating cells remains constant throughout each individual division by definition. Adding only a small fraction of symmetric divisions strongly increased the fluctuations in D. These fluctuations increased the risk of stochastic depletion, where all proliferating cells are lost, or uncontrolled exponential increase in cell number, as previously observed in simulations [9], with the probability of such events occurring increasing with ϕ (**Fig. 4B,C**). These trends are inconsistent with the symmetry between sisters we observed experimentally.

Hence, we extended the model by explicitly incorporating the observed subdivision of the crypt in a proliferative region, corresponding roughly to the stem cell niche, and non-proliferative region, corresponding to the villus domain (**Fig. 4D**). In the proliferative compartment, which has fixed size S, most divisions generate two proliferating daughter cells (α_p >0), while in the non-proliferative compartment, which has no size constraints, most divisions yield two non-proliferative daughters (α_n<0). Cell divisions in the proliferative compartment results in expulsion of the distalmost cell into the non-proliferative compartment, while neighboring cells swap positions in the proliferative compartment with rate r to include cell rearrangements. In contrast to the uniform model, where homeostasis only occurred for $\alpha=0$, the compartment model shows homeostasis with $\alpha_{p,n}\neq 0$ in either compartment. Specifically, we found that the average number of proliferating cells in the two compartments, D_p and D_n, is given by $D_p = \alpha_p\, S$ and $D_n = S\ln\left(1+\alpha_p\right)\frac{\alpha_n - \alpha_p}{\alpha_n} - \alpha_p S$, independent of the division symmetry ϕ [25]. We simulated the proliferation dynamics for different values of α_p, α_n and ϕ (**Fig. 4E,F**), where for simplicity we assumed the same ϕ in both compartments. For each combination of parameters, we varied the compartment size S so that $\langle D\rangle$=D_p+D_n=30, comparable to the number of proliferating cells per crypt in our experiments (**Materials and Methods, Fig. S4A**). For cell rearrangements, we used $r\cdot T=1$, where T is the average cell cycle time, meaning that cells

rearrange approximately once per cell cycle. For this r, our simulations reproduced the correlations in division outcome that we observed experimentally for cousins (**Fig. S5**), although we found similar results for higher r, i.e. more well-mixed compartments.

By fixing $\langle D \rangle$, all simulations maintained the same number of proliferating cells on average, but potentially differed in the magnitude of fluctuations. Indeed, we found parameter combinations that generated strong fluctuations (**Fig. 4E,F**, scenario 1) and stochastic depletion of all proliferating cells (scenario 2**).** Stochastic depletion occurred when $\alpha_p \lesssim 0.5$ (**Fig. S4B**) and implies that the existence of a stem cell niche, defined as a compartment with α>0, by itself does not guarantee homeostasis, unless its bias towards proliferation is high, $\alpha \approx 1$. For fixed α_p and α_n, we observed that fluctuations in D always decreased with more asymmetric divisions ($\phi \rightarrow 0$) (**Fig. 4E,F**, scenarios 2,3), similar to the uniform model. However, the global fluctuation minimum was strikingly different (**Fig. 4E,F**, scenario 4). Here, symmetric divisions dominated ($\phi = 1$), with all divisions generating two proliferative daughters in the proliferative compartment (α_p=1) and two non-proliferating daughters in the second other compartment (α_n=-1). Similar low fluctuations were found for a broader range of α_n, provided that $\alpha_p \approx 1$. When we quantified the magnitude of fluctuations versus the average number of proliferating cells, we found that fluctuations for the suboptimal scenarios 1-3 were larger than those expected for a Poisson birth-death process (**Fig. S2D**). In contrast, fluctuations in the optimal scenario 4 were similar to the low fluctuations we observed experimentally.

Our simulations also provided an intuitive explanation for this global minimum. A bias α_p=1 is only reached when the birth of non-proliferating cells in the proliferative compartment, by symmetric or asymmetric divisions, is fully avoided. In this limit, all cells in this compartment are proliferating, meaning that fluctuations in the proliferative compartment are entirely absent, with the only remaining fluctuations due to cells ejected from the proliferative compartment that subsequently divide in the non-proliferative compartment. Consistent with this explanation, we found that fluctuations in D increased when more symmetric divisions in the proliferative compartment generated non-proliferating daughters (scenarios 1 and 2). In conclusion, our simulations show that the dominance of symmetric divisions we observed experimentally might function to minimize fluctuations in cell proliferation.

Symmetry of proliferation is independent of Paneth cell distance

Our results raised the question how the strong symmetry in proliferative behavior between sister cells is generated. Stem cell maintenance and cell proliferation is control by signals such as Wnt and EGF, that in organoids are locally produced by Paneth cells[12, 26]. The symmetry between sister cells could therefore be explained by these sisters having a similar position relative to Paneth cells, leading them to experience a near identical environment in terms of proliferative signals. Alternatively, the proliferative behavior of sister cells could be controlled through the lineage, by their mother. In this case, symmetric proliferative behavior would even be seen in sisters that differ in position relative to Paneth cells. To differentiate between these two scenarios, we performed lysozyme staining after time-lapse imaging to retrospectively identify Paneth cells in our tracking data. Using crypt 'unwrapping' (**Fig. 1D,E**), we calculated for each cell and each time point the link distance δ to the closest Paneth cell (**Materials and Methods, Fig. S6A,B**), i.e. the number of cells between the cell of interest and its closest Paneth cell, allowing us to examine proliferative behavior as function of distance to Paneth cells.

Paneth cell-derived Wnt ligands form gradients that only penetrate 1-2 cells into the surrounding tissue [26], suggesting that the steepest gradient in proliferative signals is found in close proximity to the Paneth cell. We therefore selected all dividing mother cells directly adjacent to a Paneth cell (δ_M=0) and examined their daughters. These sister pairs varied in Paneth cell distance ($\delta_{1,2}\approx$0-2, **Fig. 5A, Fig. S6C**), with differences between sisters ($\delta_1 \neq \delta_2$) seen in 42% of pairs. We classified each sister pair as asymmetric in outcome, when only one sister continued proliferating, or symmetric (**Fig. 5B**). In the latter case, we distinguished between symmetric pairs where both sisters divided and those were both stopped proliferating. We found that most daughters cells divided again, even though a small fraction ceased division even in close proximity to Paneth cells (**Fig. 5B, Fig. S6D**) However, whether cells divided or not was fully symmetric between sister pairs, even when one cell remained adjacent to a Paneth cell (δ_1=0) while the other lost contact (δ_2>0). This also held for the few pairs where Paneth cell distance differed most between sisters (δ_1=0, δ_2=2).

When we instead examined mother cells that just lost contact with a Paneth cell (δ_M=1), we found that their offspring stopped proliferating more frequently (**Fig. 5C**). While here we did find a substantial fraction of sister pairs with asymmetric outcome, for most pairs the outcome was still symmetric (92% of pairs), even for pairs that differed considerably in relative distance to the Paneth cell. Sister pairs with asymmetric outcome occurred more frequently for pairs with different Paneth cell distance ($\delta_1 \neq \delta_2$). For these pairs, however, the non-proliferating cell was the sister closest to the Paneth cell about as often as it was the more distant (5 and 3 pairs, respectively), indicating that position relative to the Paneth cell had little impact on each sister's proliferative behavior. Overall, these results show that the symmetry of proliferative behavior between sisters did not reflect an underlying symmetry in distance to Paneth cells, thus favoring a model where this symmetry is controlled by the mother cell.

Paneth cells control proliferative bias

Even though the proliferative behavior of sisters was not explained by their relative Paneth cell distance, we found that the bias towards proliferating daughters was clearly reduced when the Paneth cell distance of the mother increased (**Fig. 5B,C**). Our simulations showed that both division symmetry and proliferative bias are important parameters in controlling fluctuations in the number of proliferating cells, with fluctuations minimized when most divisions are symmetric ($\phi\approx1$), biased strongly towards producing two proliferating daughters in one compartment ($\alpha\approx1$) and two non-proliferating daughters in the other ($\alpha\approx$-1). To compare our experiments against the model, we therefore measured the frequency of each division class as function of the mother's Paneth cell distance, averaging over all positions of the daughter cells (**Fig. 5D**). Overall, cells had a broad range of Paneth cell distances (δ=0-10). Close to Paneth cells ($\delta\leqslant1$), most divisions generated two proliferating daughters, while further away (δ>1), the majority yielded two non-proliferating cells. Asymmetry was rare and only occurred for δ=1-2. No divisions were seen for δ>5. When we used these measured frequencies to calculate α and ϕ as a function of Paneth cell distance (**Fig. 5E**), we found good agreement with the parameter values that minimized fluctuations in the model, with a compartment of strong proliferation close to Paneth cells (α=0.67, $\delta\leqslant1$) and a non-proliferative compartment beyond (α=-0.67), while almost all divisions were symmetric (ϕ=0.98).

The compartment model also predicted that the number of proliferating cells increases linearly with size S of the proliferative compartment. Above, we observed that the number of proliferating cells differed between crypts (**Fig. 2B**). We therefore examined whether variation in number of proliferating

284 cells between crypts could be explained by differences in Paneth cell number, in those crypts where
285 we identified Paneth cells by lysozyme staining (Crypts 1-4). For the crypts that maintained a constant
286 number of proliferating cells in time (Crypts 1-2), we found that differences in number of proliferating
287 cells were well explained by differences in Paneth cell number. Moreover, in crypts with increasing
288 number of proliferating cells (Crypts 3-4), we found that for Crypt 3 this change could be explained by
289 an increase of Paneth cell number, due to cell divisions that generated Paneth cell sisters. In Crypt 4,
290 however, proliferating cells increased in number without apparent Paneth cell proliferation. This crypt
291 appeared to undergo crypt fission[27] at the end of the experiment, suggesting that during fission cell
292 proliferation is altered without concomitant changes in Paneth cell number. For Crypts 1-3, the
293 relationship between number of proliferating and Paneth cells was well-fitted by a linear function (**Fig.
294 5F**), consistent with the compartment model. The fitted slope of this line indicates that one Paneth cell
295 maintains ~8 proliferating cells. This agrees with the observation in **Fig. 5D** that divisions are strongly
296 biased towards proliferation only for cells within the first and second ring of cells around each Paneth
297 cell. Taken together, these results show that Paneth cells control proliferation by tuning the
298 proliferative bias of divisions that are otherwise symmetric in proliferative outcome.

299 *In vivo* lineage tracing confirms symmetric proliferative behavior of sister
300 cells

301 Finally, we asked whether the symmetry of proliferative behavior between sister cells was also
302 observed in intestinal (stem) cells *in vivo*. Studying lineage dynamics with the high spatial and temporal
303 resolution we employed here is currently impossible *in vivo*. However, we found that clone size
304 distributions, which can be measured *in vivo*, exhibited a clear signature consistent with symmetric
305 divisions. Specifically, clone size distributions of lineages generated by the compartment model
306 showed that enrichment of even-sized clones depended strongly on a high frequency of symmetric
307 divisions (**Fig. 6A**). When we quantified clone size distributions for our organoid lineage data, by
308 counting the number of progeny of each cell at the end of a 40 h time window, while sliding that
309 window through our ~60 h data set, we indeed found that even clone sizes were strongly enriched
310 compared to odd clone sizes (**Fig. 6B**). Both for organoid and model data, we still observed odd clone
311 sizes even when virtually all divisions were symmetric in proliferative behavior. This reflected
312 variability in the cell cycle duration, with odd clone sizes typically resulting from symmetric divisions
313 where one daughter had divided, but the other not yet.

314 To measure clone size distributions in the small intestine *in vivo*, we stochastically induced heritable
315 tdTomato expression in Lgr5+ stem cells using *Lgr*5$^{\text{EGFP-ires-CreERT2}}$;R26$_{\text{LSL-tdTomato}}$ mice. We activated Cre-
316 mediated recombination by tamoxifen and examined tdTomato expression after 60 hours, similar to
317 the timescale of our organoid experiments, and imaged crypts with 3D confocal microscopy. Cre-
318 activation occurred in one cell per ~10 crypts, indicating that all labeled cells within a crypt comprised
319 a single clone. Indeed, we typically found a small number of tdTomato+ cells per crypt, of which most
320 also expressed Lgr5-GFP (**Fig. 6C**). We then counted the number of tdTomato+ cells per crypt to
321 determine the clone size distribution and found a clear enrichment of even clone sizes (**Fig. 6D**), with
322 the overall shape of the distribution similar to that measured in organoids. Overall, these results
323 indicated a dominant contribution of divisions with symmetric proliferative outcome also in the lineage
324 dynamics of Lgr5+ stem cells *in vivo*.

Discussion

Self-renewing tissues exhibit homeostasis at multiple levels, such as overall tissue morphology, total cell number and the relative frequency of different cell types. To prevent exponential growth or tissue atrophy, the birth of each proliferating cell must be balanced by the loss of another through terminal differentiation. Experiments in a range of systems indicate that this is achieved through 'population asymmetry', with each cell making the decision to proliferate or not in a stochastic manner and this balance only achieved averaged over the entire population[1, 3, 16, 20]. However, our simulations showed that even though 'population asymmetry' ensures a constant pool of proliferating cells on average, its inherently stochastic nature can cause strong fluctuations in proliferating cell number, even resulting in their full depletion (**Fig. 4**). This raises the question how these fluctuations are controlled.

We addressed this by a combined experimental and theoretical approach. We tracked all cell movements and divisions in the crypts of growing intestinal organoids, to reconstruct the full lineage of these crypts up to six generations (**Fig. 1**). These data showed that the number of proliferating cells in most organoid crypts was approximately stationary, with small, i.e. sub-Poissonian fluctuations in their number, while non-proliferating cells were born at a constant rate (**Fig. 2, Fig. S2**), an indication of homeostatic control of cell proliferation that also limits fluctuations. That intestinal organoids exhibited homeostasis is notable, as organoid culture completely lacks surrounding tissue, such as the mesenchyme, that provides key signals regulating stem cell fate and proliferation[11, 13], and shows that this form of homeostasis is inherent to the epithelium itself.

Our simulations showed that the fluctuations in proliferating cell number depended strongly on the relative proportion of divisions with symmetric proliferative outcome (either two proliferating or two non-proliferating daughters) and asymmetric outcome (one proliferating and one non-proliferating daughter), with small, sub-Poissonian cell number fluctuations only seen when most divisions had symmetric outcome (**Fig. 4**, **Fig. S2**). So far, the relative contribution of these three divisions patterns in the intestine could only be inferred indirectly from static measurements, leading to conflicting results[6, 16, 28, 29]. Here, we used direct measurements of cell dynamics in time to unambiguously identify the proliferative state of successive generations of cells. These measurements show that virtually all cell divisions (>90%) showed symmetric proliferative behavior, generating either two proliferating or two non-proliferating sisters (**Fig. 3**). Clone size distributions calculated based on our measured lineage data in organoids showed that this symmetry in proliferative behavior between sister cell gave rise to an enrichment of even clone sizes (**Fig. 6**). Using short-term lineage tracing experiments in the mouse small intestine, we found that single Lgr5+ stem cells also gave rise to more even-sized than odd-sized clones, indicating that divisions that are symmetric in proliferative behavior indeed also dominate stem cell proliferation *in vivo*.

The symmetry in proliferative behavior we observe between sister cells could arise because both cells experience a highly similar environment, in terms of proliferative signals, or rather indicate control of cell proliferation through the lineage, by the mother cell. The current models of stem cell dynamics in the intestinal crypt favor a strong role for position relative to the stem cell niche, formed in organoids by Paneth cells, and a minor role, if any, for control of cell proliferation through the lineage[6, 16, 17]. We found that sister cells exhibited symmetric proliferative behavior, even when sisters differed in distance to Paneth cells (**Fig. 5**), the sole source of proliferative Wnt signals in intestinal organoids[12].

This result implies control of proliferation by the mother cell rather than by each daughter's position in the stem cell niche. Our simulations provided a potential function for the predominance of divisions with symmetric proliferative outcome. When the tissue was subdivided into compartments of low and high cell proliferation, with the latter resembling the stem cell niche, we found that fluctuations in the number of proliferating cells were virtually eliminated, provided that cell divisions were symmetric, with all divisions generating two proliferating daughters in the niche compartment and two non-proliferating daughters outside (**Fig. 4**). Consistently, in our experiment we found that frequency of mother cells generating two proliferating rather than two non-proliferating daughters decreased with the mother's distance to the closest Paneth cell (**Fig. 5**). Taken together, our results suggest a model where differences in proliferative behavior emerges in the cell lineage over at least two generations: while a mother cell division generates two daughters with the same proliferative behavior, these daughters might subsequently generate granddaughters that differ in proliferative behavior, depending on each daughter's position relative to the Paneth cells. This is consistent with our observation that the symmetry of proliferative behavior between cousins is reduced significantly compared to sisters (**Fig. 3**).

Precise control of cell proliferation is key to homeostasis. It has been proposed that cells may sense cell density, either by chemical signals or mechanical cues, and decrease cell proliferation (known as contact inhibition) if the cell number is too high [2, 9, 30], thereby ensuring homeostasis of and minimize fluctuations in the number of proliferating cells. Here, we provide a mechanism that achieves this without explicit sensing of cell density. Instead, it relies on the dominance of divisions symmetric in proliferative behavior of the daughter cells, coupled with the organization of a tissue in a proliferative (stem and transit amplifying cell) compartment, and a non-proliferative (differentiation) compartment. Such an organization is found widely, e.g. in the skin, hair follicles, testis among others [31]. In all these tissues, homeostasis of and minimizing fluctuations in the number of proliferating and differentiated cells must be essential. Hence, we speculate that the model we propose here, which exploits proliferative symmetry between sister cells to minimize fluctuations, is conserved more broadly and relevant to diverse tissue systems.

Figures

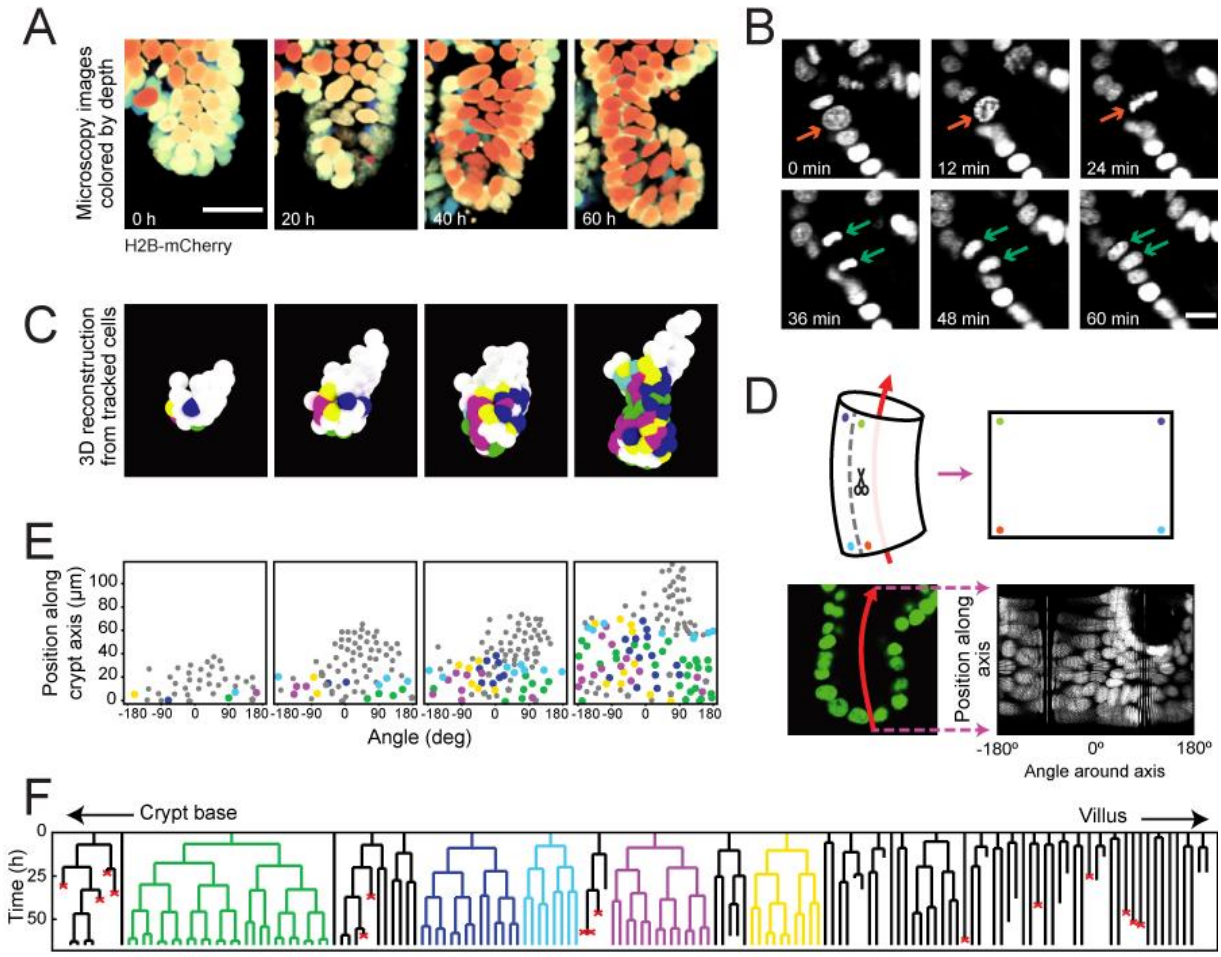

Figure 1. Time-lapse imaging and single-cell tracking of intestinal organoid crypts

(A) 3D reconstruction of an organoid expressing an H2B-mCherry reporter to visualize individual nuclei. Shown here is the crypt region, with nuclei colored by their depth along the optical axis. Scale bar is 25 µm. **(B)** Snapshots of a cell division event in a crypt. Cell divisions are distinguished by the apical migration of the nucleus followed by chromosome condensation (red arrows). After mitosis, the nuclei of the two newly born cells are displaced basally (green arrows). Scale bar is 10 µm. **(C)** 3D reconstruction of a crypt growing in time using the positions of tracked nuclei. Colors represent cells that belong to the same lineage. **(D)** Illustration of crypt unwrapping. After the crypt-villus axis is annotated (red arrow), tracked cell positions are projected onto the surface of a bent cylinder. The cylinder is then unfolded and its surface is mapped onto a two-dimensional plane defined by the distance along the axis and the angle around the axis. **(E)** Unwrapped representation of the crypt in (C), where colors represent the same lineages. **(G)** Lineage trees of cells within the crypt in (C) and colored accordingly. Cells in the initial time point are ordered according to their distance to the crypt base. Red crosses indicate cell deaths and incomplete lines indicate cells that could not be accurately traced further due to insufficient fluorescence intensity or movement outside of the field of view.

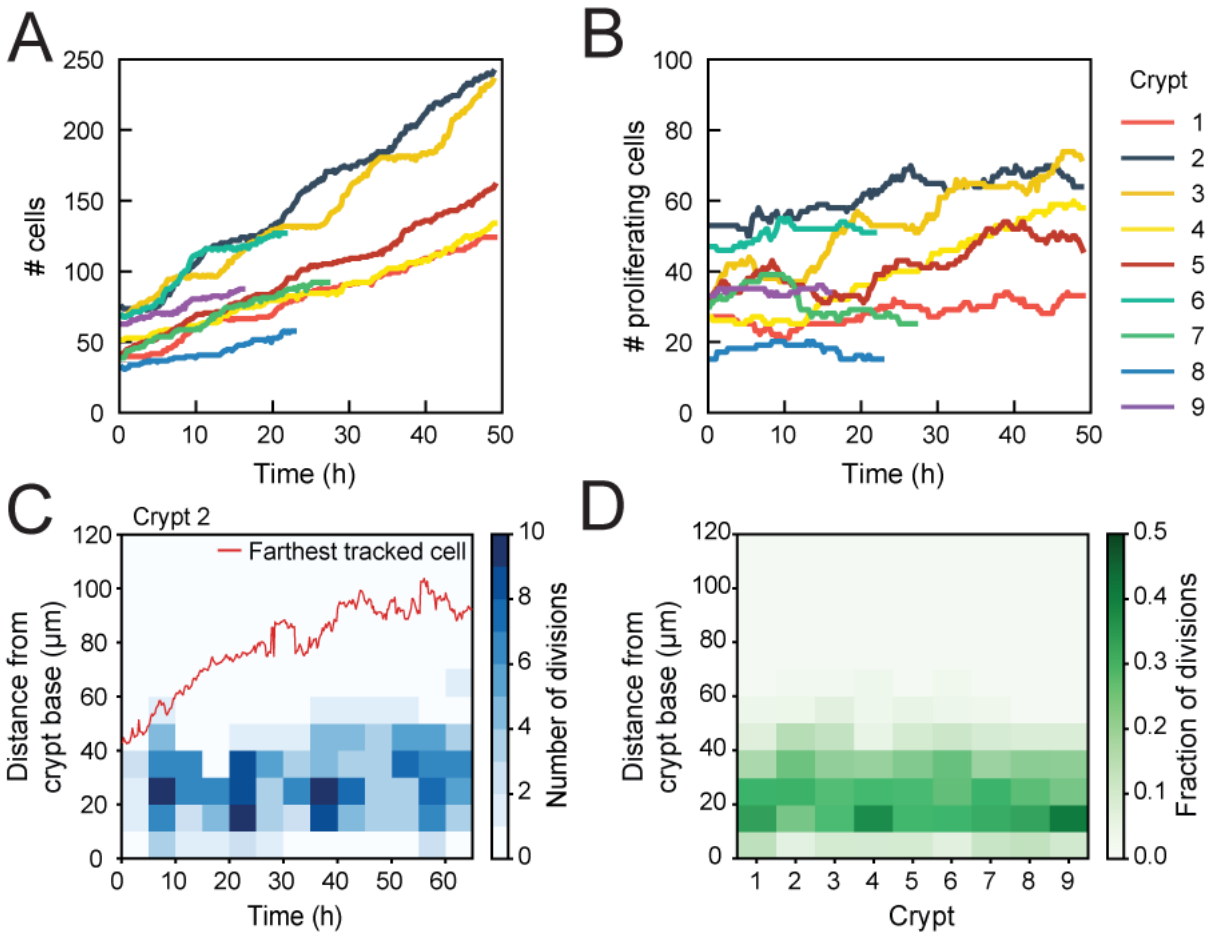

Figure 2. Control of cell divisions in intestinal organoids

(A) Total number of cell and **(B)** number of proliferating cells as a function of time for all cell lineages followed in nine tracked crypts. Note the different scale along the y-axis. Whereas total cell number increases, the number of proliferating cells remains approximately constant. The strongest increase in number of proliferating cells (~2-fold) was seen in Crypts 3 and 4. **(C)** Number of divisions that occurred at different positions along the crypt axis as a function of time in a single tracked crypt. Red line corresponds to the position of the farthest tracked cell from the crypt base at every time point. Divisions occur in a compartment close to the crypt base, whose size remain constant over time. Apical displacement of the nuclei during mitosis results in few divisions occurring at less than 10 µm from the crypt base. **(D)** Fraction of divisions that occurred at different positions along the crypt axis for all tracked crypts, averaged over the full time course. The size of the proliferative region is similar between crypts, despite differences in the total number of divisions.

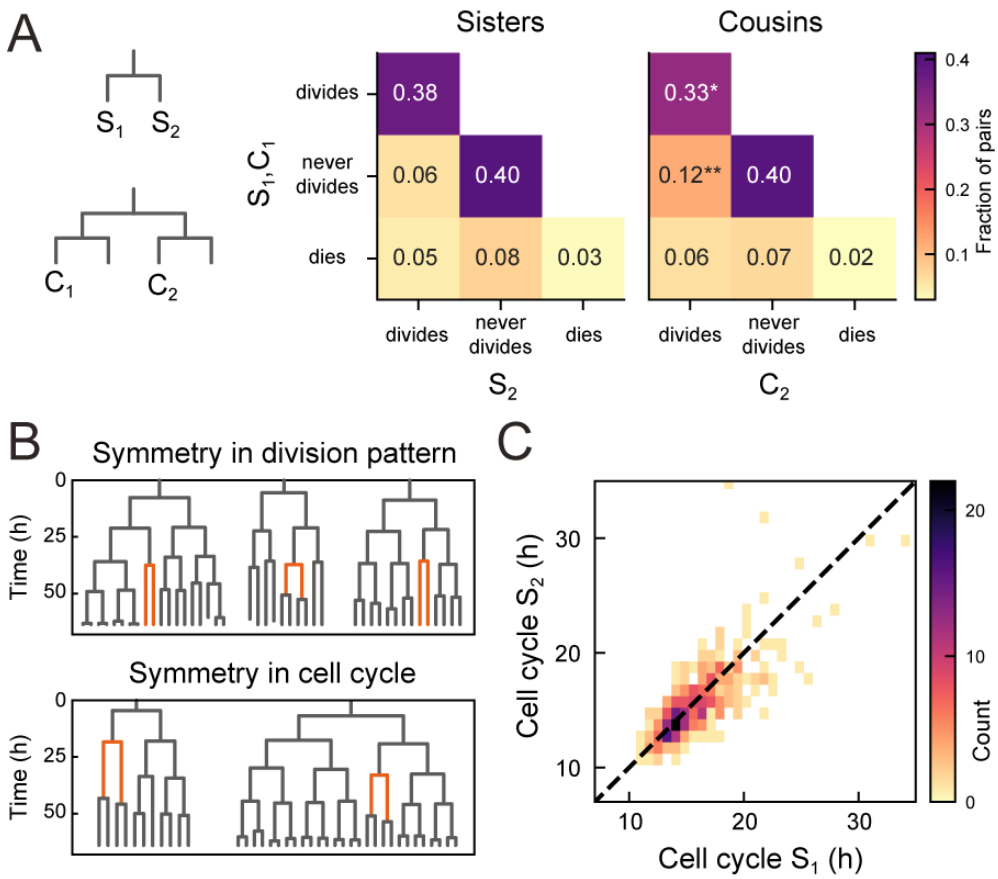

Figure 3. Symmetry of lineage dynamics between sister cells.

(A) Correlations in division patterns between sister (S_1,S_2) and cousin cells (C_1,C_2) (n=1004 and 1304 sister and cousin cell pairs). Stars indicate whether for each category the fraction measured for cousins differ from those measured for sister pairs (Chi Square Test, *P<0.05, **P<0.005). Most sister pairs show symmetrical outcomes, with most pairs consisting of sisters that either both divide or both cease dividing. Cell death occurs at low frequency and impacts sister cells asymmetrically. Symmetrical outcomes are still dominant for cousins, but the fraction of pairs that exhibited asymmetric proliferative outcomes (C_1 never divides, C_2 divides) was significantly increased in cousins compared to sisters. **(B)** Representative examples of measured lineages highlighting pairs of sister cells (orange) that differ in lineage dynamics from their more distant relatives (black), either in terms of proliferative behavior (top) or cell cycle duration (bottom). **(C)** Duration of sister cell cycles plotted against each other for pairs in which both sisters divided. Cell cycle duration is strongly correlated between sisters (R=0.80).

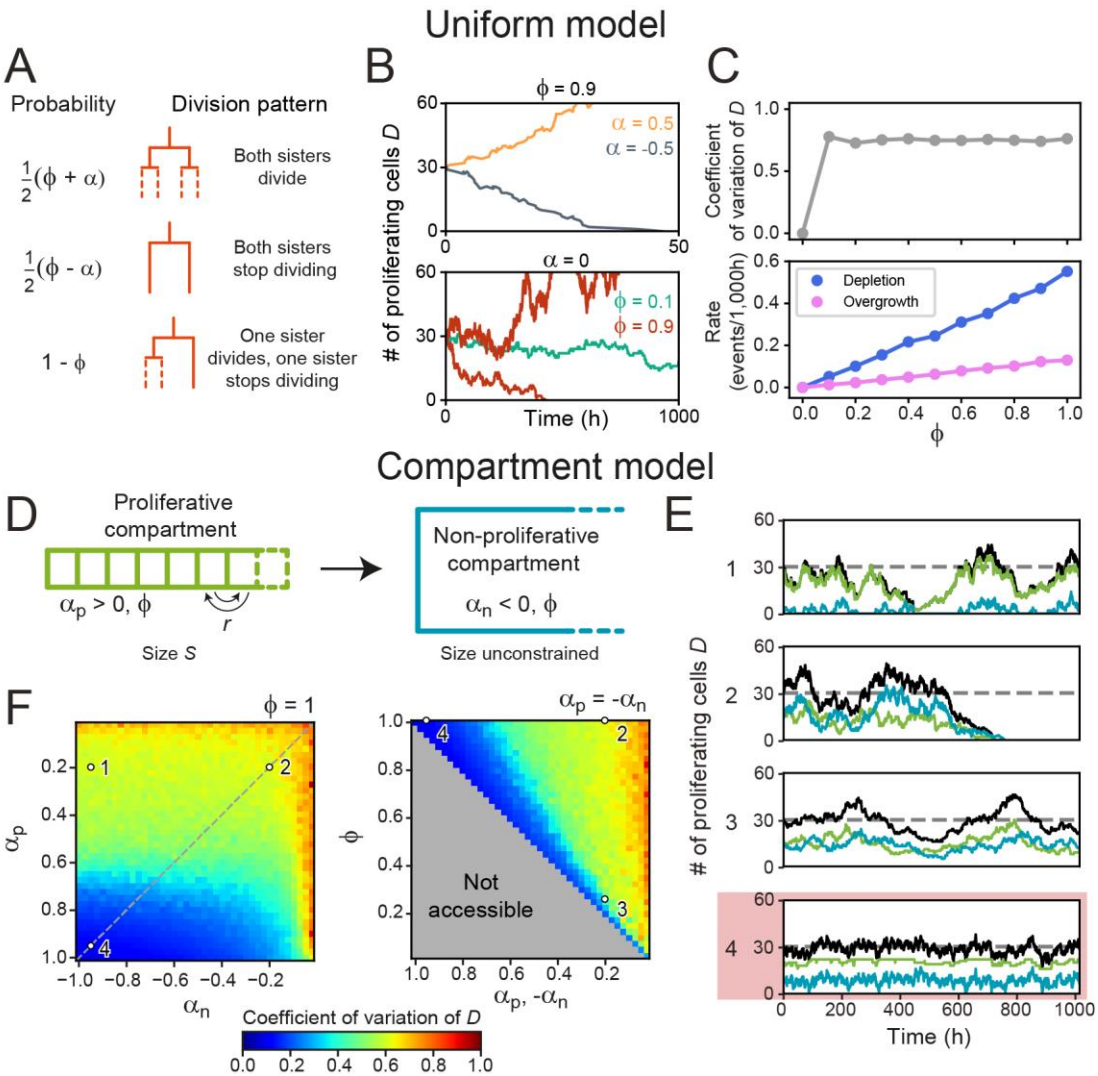

Figure 4. Cell number fluctuations in stem cell models.

(A) 'Uniform' stem cell model. Upon division, cells stochastically execute division patterns that differ in the number of proliferating daughters generated. The probability of each division pattern depends on parameters α, the average increase in the number of proliferating cells per division, and ϕ, the relative fraction between divisions with symmetric and asymmetric proliferative outcome, while the total number of cells in the tissue is unconstrained **(B)** Number of proliferating cells as function of time for simulations with different values of α (top) and ϕ (bottom). Only for α=0 does the number of proliferating cells remain constant on average, yet in this case fluctuations can cause stochastic depletion or overgrowth of proliferating cells, as shown for ϕ=0.9 (bottom). **(C)** Coefficient of variation (standard deviation divided by mean) of the number of proliferating cells D as a function of ϕ (top panel) and the probability of depletion (D=0, blue) or overgrowth ($D \geq$ 150, pink) events (bottom panel), for the 'Uniform' model with α=0. Fluctuations are minimal for ϕ=0, i.e. only asymmetric divisions. **(D)** 'Compartment' model. Cells divide according to the division patterns in (A), but now the tissue is divided in a proliferative compartment p of size S, where most divisions generate proliferating daughters, α_p>0, and a non-proliferative compartment n, where most divisions generate non-proliferating daughters, α_n<0. Both compartments have the same division symmetry ϕ. In the proliferative compartment, the total number of cells cannot exceed S, so that upon cell division the

distalmost cell (dashed square) moves into the non-proliferative compartment. Finally, cells in the proliferative compartment switch positions at rate r. **(E)** Number of proliferating cells as a function of time in the proliferative (green) and non-proliferative compartment (blue). The total number of proliferating cells (black) fluctuates around the dashed line corresponding to $\langle D \rangle$. Each panel's number refers to the parameter sets shown in (F). The parameter set with lowest fluctuations is outlined in red. **(F)** Coefficient of variation of the total number of proliferating cells D. Left panel shows the effects of varying the growth rates of both compartments when all divisions are symmetric ($\phi = 1$), and right panel of varying the degree of symmetry when both compartments have opposite growth rates (α_p=-α_n, dashed line in top panel). Numbers correspond to the simulations shown in (E). The grey region in bottom panel is inaccessible parameter space. Simulations ran with average number of proliferating cells fixed to $\langle D \rangle$= 30, corresponding to our experimental observations, and rearrangements occurring approximately once per cell cycle. Fluctuations are minimized for α_p,-α_n=1 and ϕ=1, i.e. only symmetric divisions.

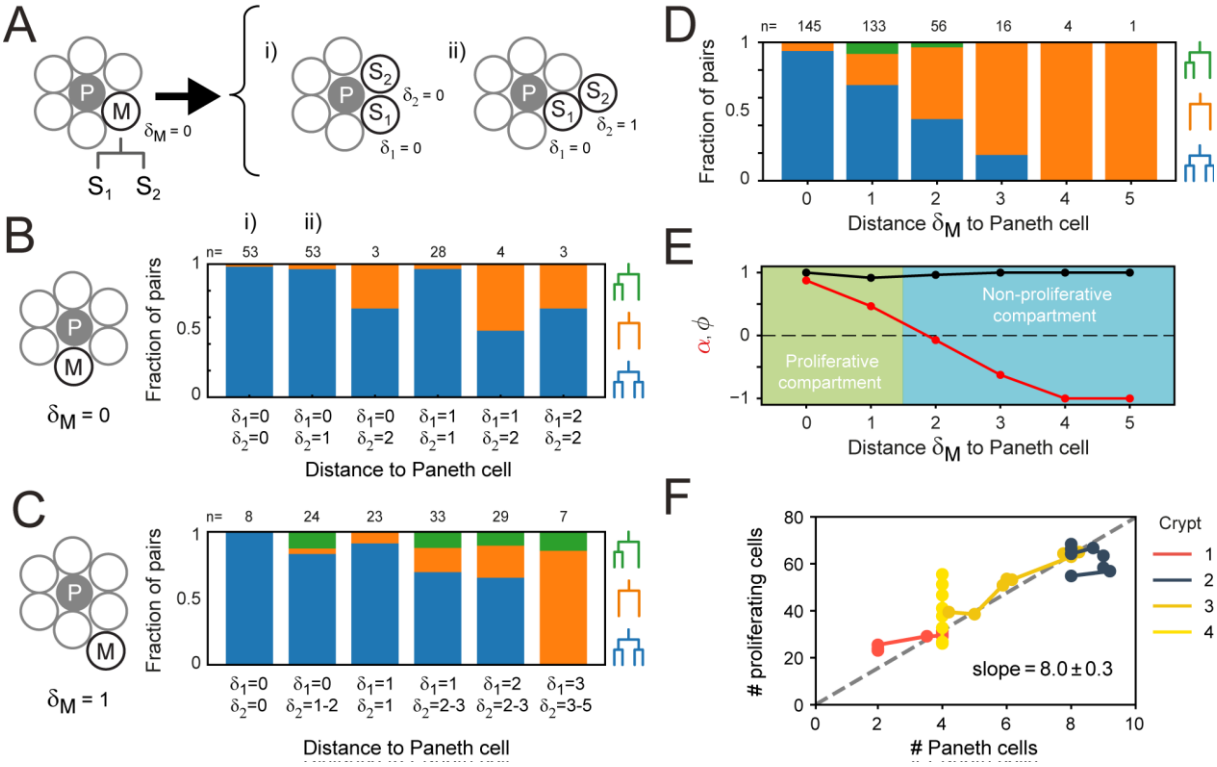

Figure 5. Impact of Paneth cell distance on proliferation.

(A) Dependence of proliferation on contact with Paneth cells. We examined cases where a mother cell (M) that touched a Paneth cell (P) divided into sister cells, S_1 and S_2, that either retained or lost Paneth cell contact. Here, the link distances δ_1 and δ_2 represents the number of cells between each sister and its closest Paneth cell. **(B)** Probability that both cells divide (blue), neither cell divides (orange) or only a single cell divides (green) for all sister pairs S_1 and S_2 of which the mother touched a Paneth cell (δ_M=0). Sister pairs exhibited full symmetry in proliferative behavior, even when distance to the Paneth cell differed between sisters ($\delta_1 \neq \delta_2$). **(C)** Same as (B) but for a mother cell positioned one cell away from the Paneth cell (δ_M=1). More daughter cells cease proliferation. While the fraction of pairs where only one sister divides increases, most sisters exhibit symmetric behavior. **(D)** Probability of each division pattern as function of Paneth cell distance of the mother cell. **(E)** Proliferative bias α and degree of symmetry ϕ as a function of Paneth cell distance. The observed values of α define a proliferative (green, $\alpha \approx 1$) and non-proliferative (blue, $\alpha < 0$) compartment, with the former corresponding approximately to the first two 'rings' of cells surrounding the Paneth cell. **(F)** Number of proliferating cells as function of Paneth cell number. Time-courses for individual crypts were divided into 5 hour intervals (markers), for which average cell numbers were calculated. Apart from Crypt 4, Paneth cell number correlated well with number of proliferating cells, even when Paneth cell number increased in time due to divisions. Dashed line is a linear fit to the data.

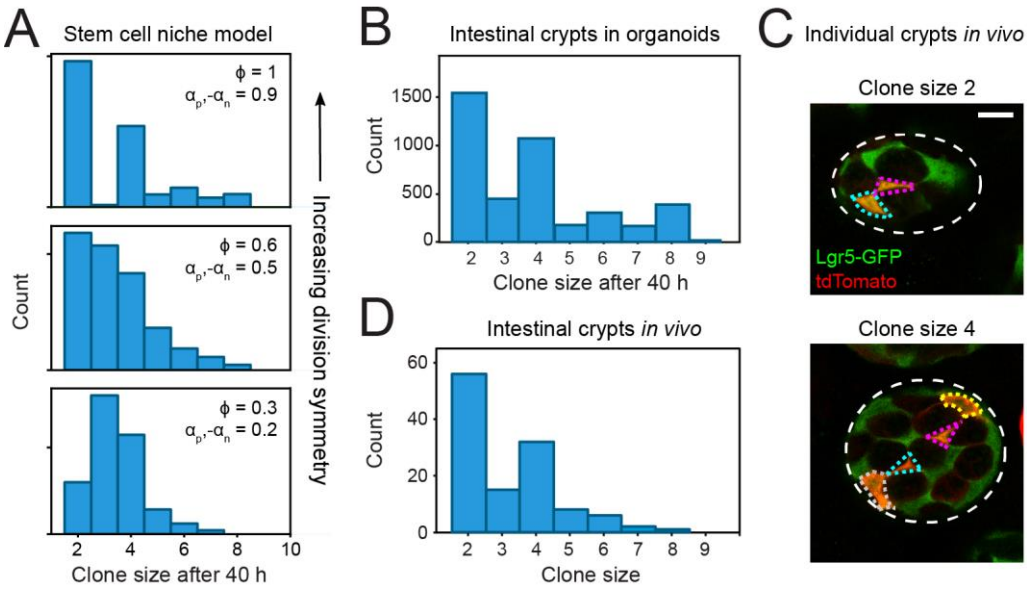

Figure 6. Clone size distributions reveal symmetry of proliferative behavior.

(A) Clone size distributions calculated for the Compartment model, for different degrees of division symmetry ϕ. Top panel corresponds to parameters that minimize fluctuations in number of proliferating cells. For high division symmetry, $\phi \approx 1$, even clone sizes are enriched compared to odd clone sizes. **(B)** Clone size distributions calculated for the lineage data obtained in organoids, for a sliding window of 40 h. Even clone sizes are enriched, consistent with the observed dominance of divisions with symmetric proliferative outcome. **(C)** Examples of individual crypts found *in vivo,* displaying clone size 2 (top) and 4 (bottom). Crypts are viewed from the bottom, with individual cells belonging to a tdTomato+ clone (red) outlined. Scale bar is 10 µm. **(D)** Clone size distributions measured *in vivo* 60 h after induction of Cre-mediated recombination in small intestinal crypts of *Lgr*5$^{\text{EGFP-ires-CreERT2}}$;R26$_{\text{LSL-tdTomato}}$ mice. Even clone sizes 2 and 4 are enriched compared to odd clone sizes 3 and 5.

Materials and methods

Organoid culture

H2B-mCherry murine intestinal organoids were a gift from Norman Sachs and Joep Beumer (Hubrecht Institute, The Netherlands). Organoids were cultured in basement membrane extract (BME, Trevingen) and overlaid with growth medium consisting of murine recombinant epidermal growth factor (EGF 50 ng/ml, Life Technologies), murine recombinant Noggin (100 ng/ml, Peprotech), human recombinant R-spondin 1 (500 ng/ml, Peprotech), n-Acetylcysteine (1 mM, Sigma-Aldrich), N2 supplement (1x, Life Technologies) and B27 supplement (1x, Life Technologies), Glutamax (2 mM, Life Technologies), HEPES (10mM, Life Technologies), Penicilin/Streptomycin (100 U/ml 100 µg/ml, Life Technologies) in Advanced DMEM/F-12 (Life Technologies). Organoid passaging was performed by mechanically dissociating crypts using a narrowed glass pipette.

Time-lapse imaging

Mechanically dissociated organoids were seeded in imaging chambers one day before the start of the time-lapse experiments. Imaging was performed using a scanning confocal microscope (Nikon A1R MP) with a 40x oil immersion objective (NA = 1.30). 30 z-slices with 2 µm step size were taken per organoid every 12 minutes. Experiments were performed at 37°C and 5% CO_2. Small but already formed crypts that were budding perpendicularly to the objective were selected for imaging.

Fluorescent staining

After time-lapse imaging, organoids were fixed with 4% formaldehyde (Sigma) at room temperature for 30 minutes. Next, they were permeabilized with 0.2% Triton-X-100 (Sigma) for one hour at 4°C and blocked with 5% skim milk in TBS at room temperature for one hour. Subsequently, organoids were incubated in blocking buffer containing primary antibody (rabbit anti-lysozyme 1:800, Dako #A0099) overnight at 4°C, and then incubated with secondary antibody (anti-rabbit conjugated to Alexa Fluor©405 1:1,000, Abcam #ab175649) at room temperature for one hour. Afterwards, they were incubated with wheat germ agglutinin (WGA) conjugated to CF©488A (5 µg/ml Biotium) at room temperature for two hours, followed by incubation with RedDot™1 Far-Red Nuclear Stain (1:200, Biotium) at room temperature for 20 minutes. Finally, organoids were overlaid with mounting medium (Electron Microscopy Sciences). The procedure was performed in the same imaging chambers used for time-lapse imaging in order to maintain organoids in the same position. Imaging was performed with the same microscope as previously described. Note that WGA stains both Paneth and Goblet cells, but the lysozyme staining allowed the unequivocal distinction between them.

Single-cell tracking

Cells were manually tracked by following the center of mass of their nuclei in 3D space and time using custom-written image analysis software. Each cell was assigned a unique label at the start of the track. For every cell division, we noted the cell labels of the mother and two daughter cells, allowing us to reconstruct lineage trees. We started by tracking cells that were at the crypt bottom in the initial time point and progressively tracked cells positioned towards the villus region until we had covered all cells within the crypt that divided during the time-lapse recording. We then tracked at least one additional row of non-dividing cells positioned towards the villus region. Cell deaths were identified either by the

extrusion of whole nuclei into the organoid lumen or by the disintegration of nuclei within the epithelial sheet. Only crypts that grew approximately perpendicularly to the imaging objective and that did not undergo crypt fission were tracked. Data was discarded when a large fraction (> 25%) of the cells move out of the imaged volume.

Classifying cell state

To classify cells as either proliferating or non-proliferating, we followed the following procedure. Defining proliferating cells was straightforward, as their division could be directly observed. As for non-proliferating cells, we applied two criteria. Either, cells were tracked for at least 30 hours without dividing. This was based on our observation that we found no cells that divided more than 30 hours after their birth (**Fig. S3**). Alternatively, if we were unable to track a cell for 30 hours, either because it went out of the field of view or because it was born soon before the end of the time-lapse experiment, we defined it as non-proliferating if its last recorded position along the crypt axis was higher than 60 µm, as almost no divisions were observed beyond this distance (**Fig. 2**). Dying cells were identified by their ejection from the epithelium. All other cells were classified as undetermined and were not included in the analysis.

Estimation of crypt growth rate

To estimate an effective growth rate from the time dynamics of the total cell number and number of proliferating cells for each individual crypt, we used the 'Uniform' model as defined in the main text. The resulting dynamics of the number of proliferating and non-proliferating cells, D and M, is given by $\frac{dD}{dt}=\frac{\alpha}{T}D$ and $\frac{dM}{dt}=\frac{1-\alpha}{T}D$, where α is the exponential growth rate and T is the average cell cycle duration. Solving these differential equations yields $D(t) = D(0)\exp(\frac{\alpha t}{T})$ and $N(t) = M(0)$-$\frac{1-\alpha}{\alpha}D(0)+\frac{D(0)}{\alpha}\exp(\frac{\alpha t}{T})$ for the total number of cells, where N=D+M. We then fitted $N(t)$ and $D(t)$ to the experimental data in **Fig. 2A,B**, using a single value of the fitting parameter α for each crypt and the experimentally determined value of T=16.2 h.

Crypt unwrapping

At every time point the crypt axis was manually annotated in the xy plane at the z position corresponding to the center of the crypt, since tracked crypts grew perpendicularly to the objective. Three to six points were marked along the axis, through which a spline curve $\boldsymbol{s}(r)$ was interpolated. Then, for each tracked cell i we determined its position along the spline by finding the value of r that minimized the distance d between the cell position $\boldsymbol{x}_i$and the spline, i.e. $d(r_i) = \min_{\mathrm{r}} |\boldsymbol{s}(r) - \boldsymbol{x}_i|$. At each time point, the bottom-most cell of the crypt, i.e. that with the lowest value of r_i, was defined as position zero. Thus, the position along the axis p_i for cell i was defined as $p_i = r_i - \min_i(r_i)$. To determine the angle around the axis θ_i for cell i, we considered a reference vector $\boldsymbol{u}$ pointing in the direction of the imaging objective, given by $\boldsymbol{u} = (0,0,-1)$, and the vector $\boldsymbol{v}_i = \boldsymbol{x}_i - \boldsymbol{s}(r_i)$ defined by the position of the cell $\boldsymbol{x}_i$ and the position of minimum distance along the spline $\boldsymbol{s}(r_i)$. Then, the angle is given by $\theta_i = \operatorname{acos}(\boldsymbol{u} \cdot \boldsymbol{v}_i/uv)$.

Distance to Paneth cells

586 To estimate the distance between cells we used the following approach. For each cell at each time
587 point we found the five closest cells within a 15 µm radius, which became the edges in a graph
588 representation of the crypt (**Fig. S6**). These values were chosen because a visual inspection revealed
589 an average nucleus size of 10 µm and an average of five neighbors per cell. This graph was then used
590 to define the edge distance of a cell to the nearest Paneth cell. At every time point during the lifetime
591 of that cell, the minimum number of edges required to reach the nearest Paneth cell was recorded.
592 The edge distance is then defined as the number of edges minus one. For example, a neighbor cell of
593 a Paneth cell (1 edge) has a distance of zero. When the edge distance of a cell to a Paneth cell varied
594 in time, we used the mode of its distance distribution, i.e. the most frequently-occuring value, as
595 recorded during its lifetime.

596 *In vivo* clonal tracing

597 All experiments were carried out in accordance with the guidelines of the animal welfare committee
598 of the Netherlands Cancer Institute. *Lgr*5$^{EGFP\text{-}ires\text{-}CreERT2}$;R26$_{LSL\text{-}tdTomato}$ double heterozygous male and
599 female mice (Bl6 background) were housed under standard laboratory conditions and received
600 standard laboratory chow and water ad libitum prior to start of the experiment. 60 hours before
601 sacrifice, mice received an intraperitoneal injection with 0.05 mg tamoxifen (Sigma, T5648; dissolved
602 in oil) resulting in maximally 1 labeled cell per ~10 crypts. After sacrifice, the distal small intestine was
603 isolated, cleaned and flushed with ice cold PBSO, pinned flat and fixed for 1.5 hours in 4% PFA (7.4 pH)
604 at 4°C. The intestine was washed in PBT (1% Tween-20) for 10 min at 4°C after which it was cut into
605 pieces of ~2 cm and transferred to a 12 well plate for staining. The pieces were permeabilized for 5
606 hours in 3% BSA and 0.8% Triton X-100 in PBSO and stained overnight at 4°C using anti-RFP (Rockland,
607 600-401-379) and anti-GFP (Abcam, ab6673) antibodies. After 3 times 30 min washes at 4°C in 0.1%
608 Triton X-100 and 0.2% BSA in PBSO, the pieces were incubated with Alexa fluor Donkey anti rabbit 568
609 (Invitrogen, A10042) and Alexa fluor Donkey anti goat 488 (Invitrogen, A11055) secondary antibodies
610 overnight at 4°C. After an overnight wash in PBT, the pieces were incubated with DAPI (Thermo Fisher
611 Scientific, D1306) for 2 hour and subsequently washed in PBS for 1 hour at 4°C. Next, the intestinal
612 pieces were cleared using 'fast light-microscopic analysis of antibody-stained whole organs' (FLASH)
613 described in Messal et al.[18]. In short, samples were moved to an embedding cassette and dehydrated
614 in 30%, 75%, 2x 100% MetOH for 30 min each at RT. Subsequently, samples were put into MetOH in a
615 glass dish and immersed in methyl salicylate diluted in MetOH: 25%, 75%, 2x 100% methyl salicylate
616 (Sigma-Aldrich) 30 min each at RT protected from light. Samples were mounted in methyl salicylate in
617 between two glass coverslips and images were recorded using an inverted Leica TCS SP8 confocal
618 microscope. All images were collected in 12 bit with 25X water immersion objective (HC FLUOTAR L
619 N.A. 0.95 W VISIR 0.17 FWD 2.4 mm). Image analysis was carried out independently by two persons.
620 Afterwards, all discrepancies between both datasets were inspected, resulting in a single dataset. Each
621 biologically stained cell was annotated once in the 3D-dimensional image. Different cells in the same
622 crypt were marked as belonging to the same crypt, which is necessary to calculate the clone size for
623 that crypt. Only crypts that were fully visible within the microscopy images were analyzed.

624 Computational model

625 Simulations were initialized by generating a collection of proliferating cells, each belonging to either
626 the proliferative or non-proliferative compartment. For each parameter combination, the initial
627 number of proliferating cells assigned to each compartment was obtained by rounding to the closest

integer the values given by the equations for D_n and D_d in the main text. When the initial number of proliferating cells in the proliferative compartment was lower than the compartment size S, they were randomly distributed over the compartment, with the remaining positions taken up by non-proliferating cells in order to fill the compartment. Each proliferating cell c that was generated was assigned a current age A_c and a cell cycle time C_c, i.e. the age at which the cell will eventually divide. The current age was obtained by randomly drawing a number from an interval ranging from 0 hours to the mean cell cycle time (16.15 hours) obtained from experimental data, while the cell cycle was obtained by drawing a random number from a skew normal distribution, which was fitted to the experimental distribution of cell cycle times as shown in **Fig. S3**.

Simulations were performed by iterating the following routine over time, until a total simulation time $T = 10^6$ h was reached. At each iteration i, we found the cell c_i that was due to divide next, and a time step Δt_i was defined by the time remaining for this cell to divide, i.e. $\Delta t_i = \min_c(C_c - A_c)$. Then, the ages of all proliferating cells were updated and the division of cell c_i was executed. This was done by randomly choosing one of the three division modes defined in **Fig. 4C**, according to the probabilities determined by the parameters α and ϕ of the compartment to which the cell belonged. Any proliferating daughters that were born were initialized with age zero and a random cell cycle time drawn as described before. For the two-compartment model, if the proliferating cell belonged to the proliferative compartment, the distalmost cell within this compartment was transferred to the non-proliferative compartment. Finally, the number of proliferating and non-proliferating cells in each compartment was updated accordingly. Cell rearrangements were implemented as follows. For each iteration i, with time step Δt_i, we drew the number of cell rearrangements from a Poisson distribution with mean $(r \cdot S)\Delta t_i$, where r is the rearrangement rate per cell. We then implemented each individual rearrangement by randomly selecting a cell at position $j \in (0, S\text{-}1)$ and swapping it with the cell at position $j+1$. For a 'well-mixed' proliferative compartment, $r{\cdot}T \gg 1$, cousin pairs showed asymmetric outcome as often as symmetric outcome (**Fig. S4**), in contrast to our experimental observations (**Fig. 3A**). In contrast, for infrequent cell rearrangement, $r{\cdot}T{=}1$, cells are expelled from this compartment close together in time are closely related by lineage, leading to correlations in division outcome between cousins that reproduced those observed experimentally (**Fig. S4, Fig. 3A**).

For some parameter values, simulations were ended earlier than the total time T. This occurred when no proliferating cells were left in either compartment (defined as a depletion event), or when the number of proliferating cells reached an arbitrarily set maximum limit of five times its initial value (defined as an overgrowth event, occurring only in the one-compartment model). In these cases, simulations were restarted until a total simulation time T was reached, and the total number of events was recorded. Thus, the rate of depletion or overgrowth refers to the number of times simulations had to be restarted for each value of ϕ divided by the total simulation time.

To obtain statistics regarding fluctuations on the number of proliferating cells D through time, at each iteration i we kept track of the number of proliferating cells in the proliferative compartment d_i^p and in the non-proliferative compartment d_i^n. With these quantities, we could compute the standard deviation σ of D according to $\sigma^2 = \langle D^2 \rangle - \langle D \rangle^2$. Given that $D = D_p + D_n$, where D_p and D_n are the number of proliferating cells in the proliferative and non-proliferative compartments, σ can be expressed as $\sigma^2 = \langle D_p^2 \rangle - \langle D_p \rangle^2 + \langle D_n^2 \rangle - \langle D_n \rangle^2 + 2\langle D_p D_n \rangle - 2\langle D_p \rangle \langle D_n \rangle$, where $\langle D_{p,n} \rangle = \sum_i \frac{d_i^{p,n} \Delta t_i}{T}$, $\langle D_{p,n}^2 \rangle = \sum_i \frac{(d_i^{p,n})^2 \Delta t_i}{T}$ and $\langle D_p D_n \rangle = \sum_i \frac{d_i^p d_i^n \Delta t_i}{T}$.

670 ## References

671 1. Simons, B.D. and H. Clevers, *Strategies for homeostatic stem cell self-renewal in adult tissues.*
672 Cell, 2011. **145**(6): p. 851-62.
673 2. Lander, A.D., et al., *Cell lineages and the logic of proliferative control.* PLoS Biol, 2009. **7**(1): p.
674 e15.
675 3. Clayton, E., et al., *A single type of progenitor cell maintains normal epidermis.* Nature, 2007.
676 **446**(7132): p. 185-9.
677 4. Klein, A.M., et al., *Kinetics of cell division in epidermal maintenance.* Phys Rev E Stat Nonlin
678 Soft Matter Phys, 2007. **76**(2 Pt 1): p. 021910.
679 5. Klein, A.M. and B.D. Simons, *Universal patterns of stem cell fate in cycling adult tissues.*
680 Development, 2011. **138**(15): p. 3103-11.
681 6. Lopez-Garcia, C., et al., *Intestinal stem cell replacement follows a pattern of neutral drift.*
682 Science, 2010. **330**(6005): p. 822-5.
683 7. Rué, P. and A. Martinez Arias, *Cell dynamics and gene expression control in tissue homeostasis*
684 *and development.* Mol Syst Biol, 2015. **11**(1): p. 792.
685 8. Feller, W., *Die grundlagen der volterraschen theorie des kampfes ums dasein in*
686 *wahrscheinlichkeitstheoretischer behandlung.* Acta Biotheoretica, 1939. **5**(1): p. 11-40.
687 9. Sun, Z. and N.L. Komarova, *Stochastic modeling of stem-cell dynamics with control.*
688 Mathematical biosciences, 2012. **240**(2): p. 231-240.
689 10. Gehart, H. and H. Clevers, *Tales from the crypt: new insights into intestinal stem cells.* Nat Rev
690 Gastroenterol Hepatol, 2019. **16**(1): p. 19-34.
691 11. Farin, H.F., J.H. Van Es, and H. Clevers, *Redundant sources of Wnt regulate intestinal stem cells*
692 *and promote formation of Paneth cells.* Gastroenterology, 2012. **143**(6): p. 1518-1529.e7.
693 12. Sato, T., et al., *Paneth cells constitute the niche for Lgr5 stem cells in intestinal crypts.* Nature,
694 2011. **469**(7330): p. 415-8.
695 13. Shoshkes-Carmel, M., et al., *Subepithelial telocytes are an important source of Wnts that*
696 *supports intestinal crypts.* Nature, 2018. **557**(7704): p. 242-246.
697 14. Scoville, D.H., et al., *Current view: intestinal stem cells and signaling.* 2008. **134**(3): p. 849-864.
698 15. Winton, D. and B. Ponder, *Stem-cell organization in mouse small intestine.* Proceedings of the
699 Royal Society of London. Series B: Biological Sciences, 1990. **241**(1300): p. 13-18.
700 16. Snippert, H.J., et al., *Intestinal crypt homeostasis results from neutral competition between*
701 *symmetrically dividing Lgr5 stem cells.* Cell, 2010. **143**(1): p. 134-44.
702 17. Ritsma, L., et al., *Intestinal crypt homeostasis revealed at single-stem-cell level by in vivo live*
703 *imaging.* Nature, 2014. **507**(7492): p. 362-365.
704 18. Sato, T., et al., *Single Lgr5 stem cells build crypt-villus structures in vitro without a mesenchymal*
705 *niche.* 2009. **459**(7244): p. 262-265.
706 19. Doupé, D.P., et al., *A single progenitor population switches behavior to maintain and repair*
707 *esophageal epithelium.* Science, 2012. **337**(6098): p. 1091-3.
708 20. Klein, A.M., et al., *Mouse germ line stem cells undergo rapid and stochastic turnover.* Cell Stem
709 Cell, 2010. **7**(2): p. 214-24.
710 21. Teixeira, V.H., et al., *Stochastic homeostasis in human airway epithelium is achieved by neutral*
711 *competition of basal cell progenitors.* Elife, 2013. **2**: p. e00966.
712 22. Ragkousi, K. and M.C. Gibson, *Cell division and the maintenance of epithelial order.* J Cell Biol,
713 2014. **207**(2): p. 181-8.
714 23. Swain, P.S., *Lecture notes on stochastic models in systems biology.* arXiv preprint
715 arXiv:1607.07806, 2016.
716 24. Corominas-Murtra, B., et al., *Stem cell lineage survival as a noisy competition for niche access.*
717 Proc Natl Acad Sci U S A, 2020. **117**(29): p. 16969-16975.
718 25. Kok, R.N.U., S.J. Tans, and J.S. van Zon, *Minimizing cell number fluctuations in self-renewing*
719 *tissues with a stem cell niche.* bioRxiv, 2022: p. 2022.03.10.483777.

720 26. Farin, H.F., et al., *Visualization of a short-range Wnt gradient in the intestinal stem-cell niche.*
721 Nature, 2016. **530**(7590): p. 340-3.
722 27. Langlands, A.J., et al., *Paneth Cell-Rich Regions Separated by a Cluster of Lgr5+ Cells Initiate*
723 *Crypt Fission in the Intestinal Stem Cell Niche.* PLoS Biol, 2016. **14**(6): p. e1002491.
724 28. Itzkovitz, S., et al., *Optimality in the development of intestinal crypts.* Cell, 2012. **148**(3): p. 608-
725 19.
726 29. Sei, Y., et al., *Asymmetric cell division-dominant neutral drift model for normal intestinal stem*
727 *cell homeostasis.* 2019. **316**(1): p. G64-G74.
728 30. Eisenhoffer, G.T. and J. Rosenblatt, *Bringing balance by force: live cell extrusion controls*
729 *epithelial cell numbers.* Trends Cell Biol, 2013. **23**(4): p. 185-92.
730 31. Li, L. and T. Xie, *Stem cell niche: structure and function.* Annu Rev Cell Dev Biol, 2005. **21**: p.
731 605-31.

732

733

Supporting Figures

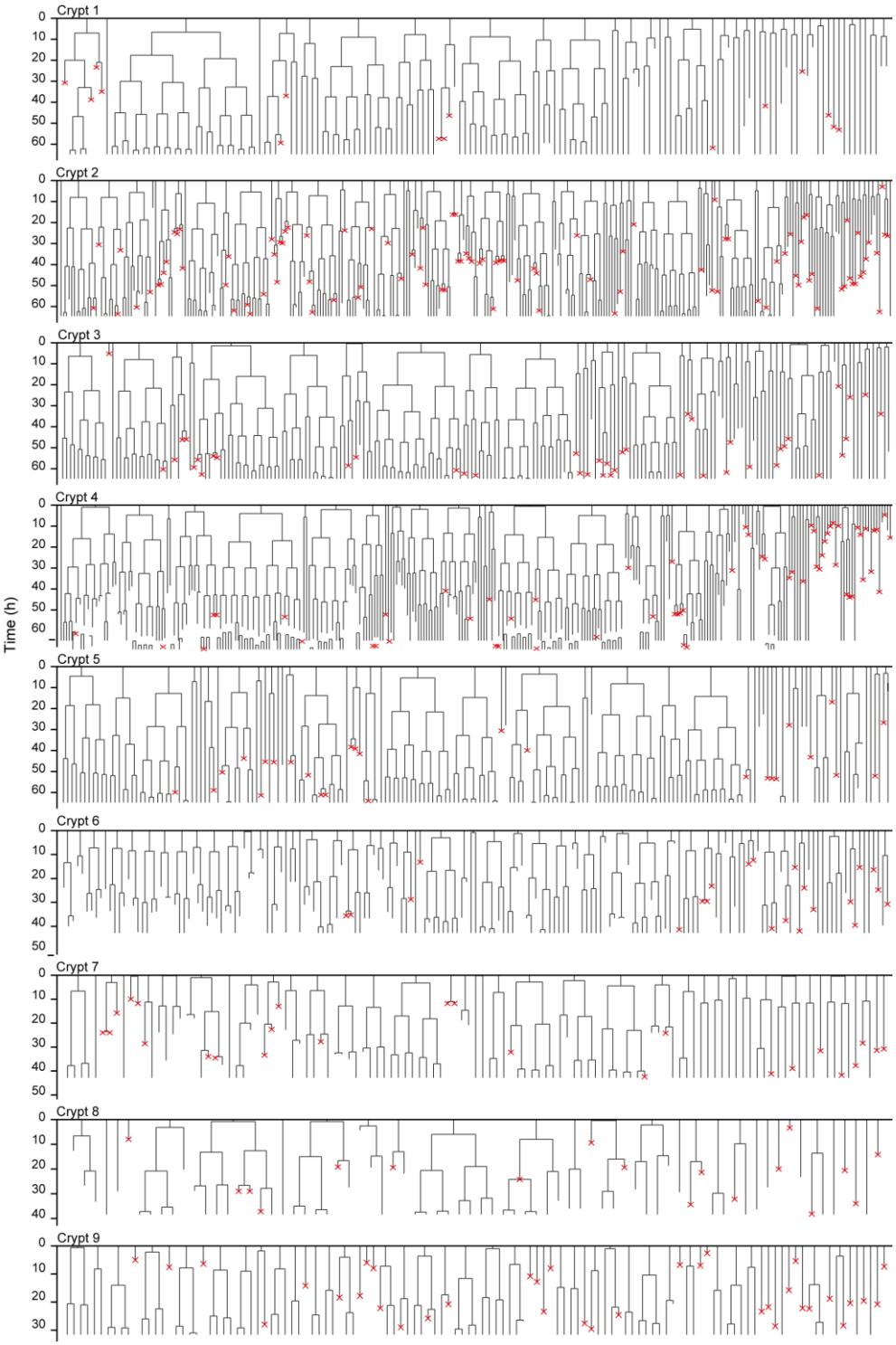

Figure S1. Lineage trees of all tracked cells

Lineage trees of cells tracked in nine different crypts. Cells in the initial time point are ordered according to their distance to the crypt base. Red crosses indicate cell deaths and incomplete lines indicate cells that could not be accurately traced further due to insufficient fluorescence intensity or movement outside of the field of view.

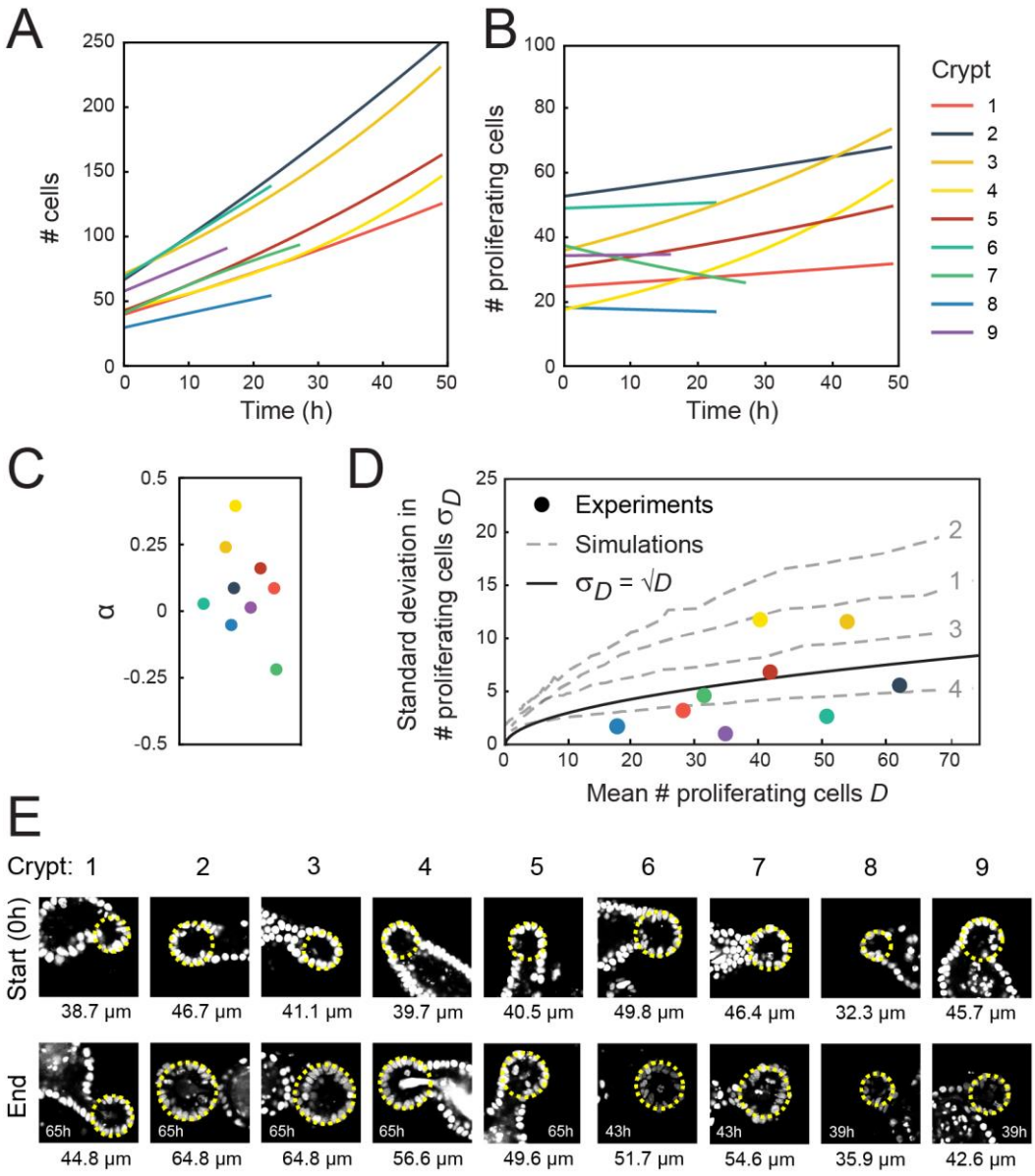

Figure S2. Crypt growth and heterogeneity

(A),(B) Fits of a simple cell proliferation model (**Materials and Methods**) to the experimental data in **Fig. 2A,B**. Each fit to the total number of cells (A) and number of proliferating cells (B) yields a single fitted value of the exponential growth rate α. **(C)** Fitted values of α, with the color of each marker corresponding to the crypts in (A),(B). Two crypts exhibited significant growth (crypts 3 and 4, $\alpha \geqslant 0.25$) while one crypt show decay in proliferating cell number (crypt 7, α=-0.25). For this reason, the reported average growth rate in the main text excluded crypts 3,4 and 7. Including crypt 7 yields $\alpha = 0.0 \pm 0.1$. **(D)** Standard deviation of the number of proliferating cells, σ_D, versus the average, D, for each crypt, with color indicating crypts as in (A),(B). Black line shows the relationship expected for a Poisson birth-death process, $\sigma_D = \sqrt{D}$. For crypts that exhibited growth (crypt 3 and 4), σ_D was larger than a Poisson process, while other crypts showed fluctuations close to or below what was expect for a Poisson process, implying that fluctuations were limited by some form of homeostatic control. Grey dashed lines show the same analysis for simulations of the 'Compartment' model (**Fig. 4D)**, with individuals lines corresponding to the different scenarios 1-4 (indicated in grey) in **Fig. 4E,F**. For the

suboptimal scenarios 1-3, fluctuations are larger than Poissonian, while the optimal scenario 4 reproduced the low fluctuations observed experimentally. **(E)** Fluorescence images of analyzed crypts 1-9 at the start and end of the experiment. Duration of the experiment is indicated in each 'end' panel. Diameter of the crypt at the start and end of the experiment is calculated by overlaying a circle (yellow line) over the z-slice at the center of the crypt. Overall, crypts display heterogeneity both in initial crypt size and growth of crypt diameter.

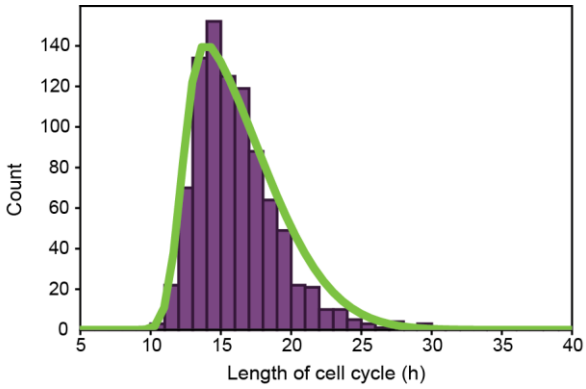

Figure S3. Cell cycle distribution

Histogram of cell cycle times of all tracked dividing cells. Green line represents a skew normal distribution fitted to the data, with parameters: shape = 6.1, location = 12.2 h, and scale = 5.2 h.

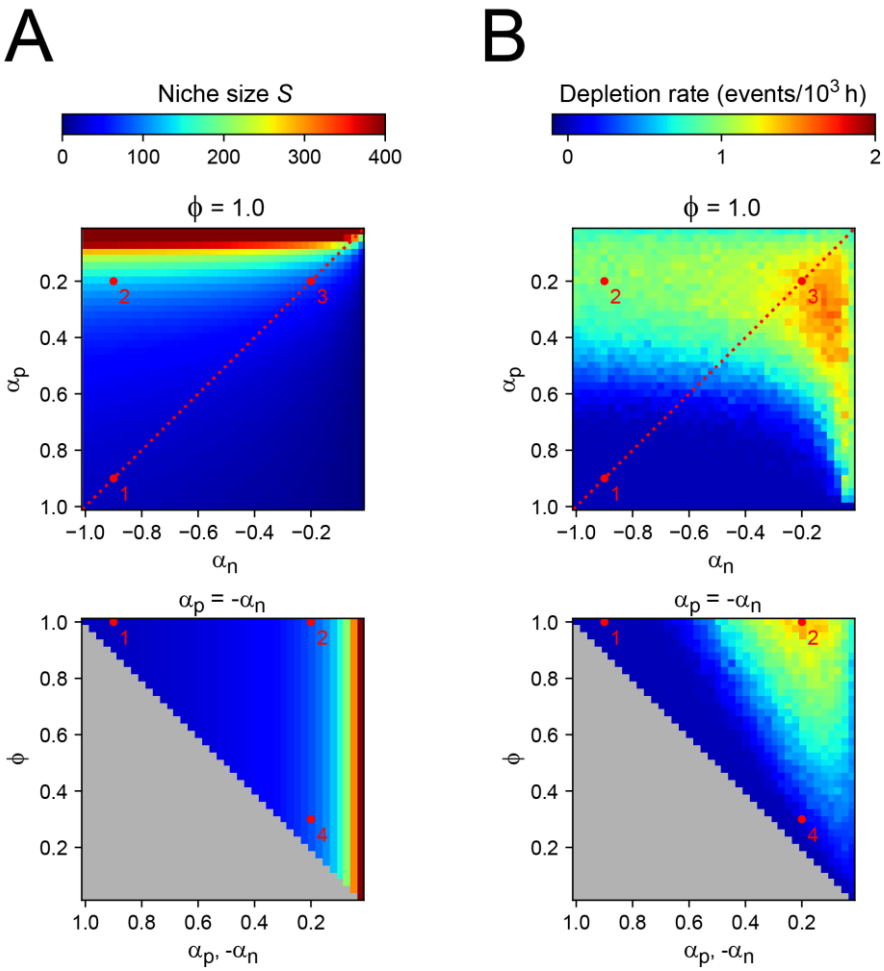

Figure S4. Two-compartment model

(A) Number of cells S in the proliferative compartment, as function of model parameters in the Compartment model. Top panel shows the effects of varying the bias towards proliferative daughters of the proliferative and non-proliferative compartments (α_p and α_n, respectively) when all divisions are symmetric ($\phi = 1$), and bottom panel shows the effects of varying the degree of symmetry when these compartments have opposite growth rates ($\alpha_p = -\alpha_n$, dashed line in top panel). The grey region in bottom panel corresponds to inaccessible parameter space. Numbers correspond to the parameter sets highlighted in Fig. 4 in the main text. **(B)** Rate at which proliferating cells were depleted. Every time a simulation ended due to depletion, i.e. all remaining cells are non-proliferating, a new simulation was started until a total simulation time of 10^6 hours was reached. Thus, the rate refers to the number of times simulations had to be restarted for each value of the parameters divided by the total simulation time. Spontaneous overgrowth was only observed in cases where α_p and α_n are both close to 0, in which case the rate was low (~10^{-5} h^{-1}).

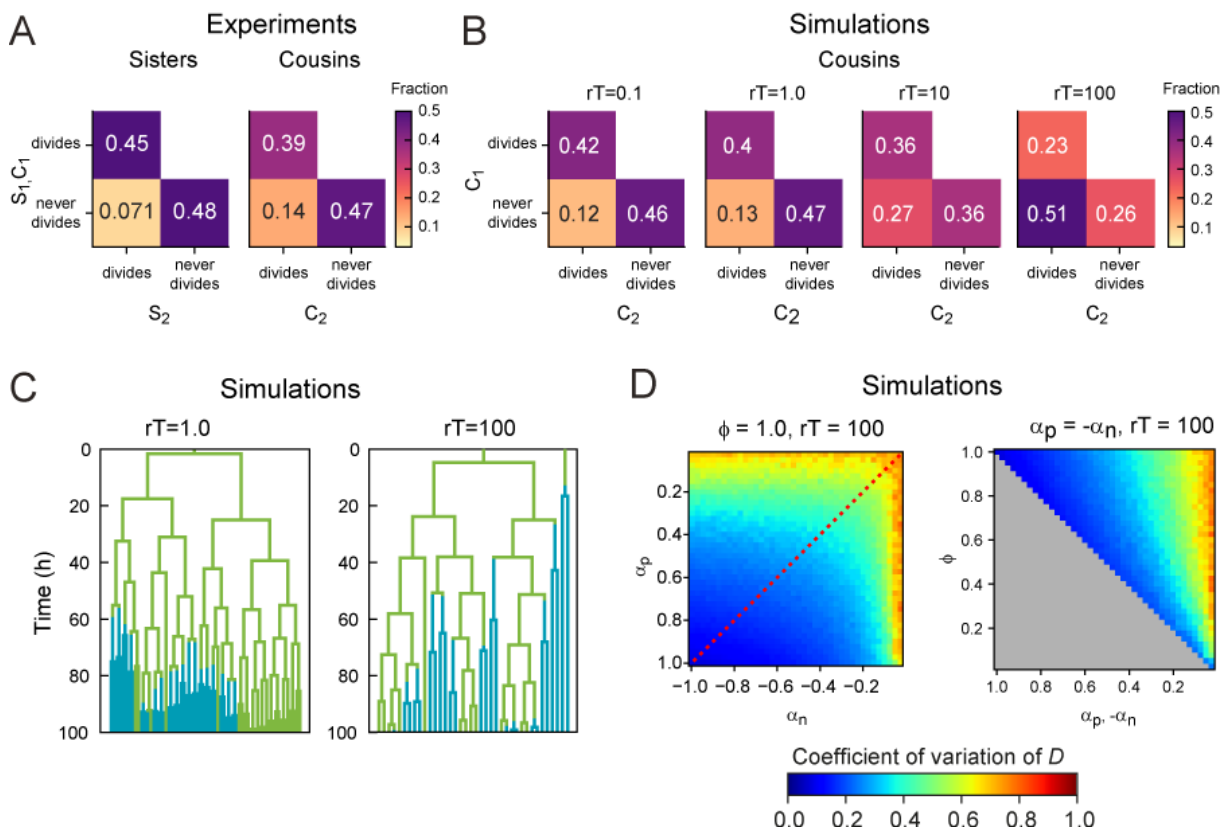

Figure S5. Dependence of lineage dynamics on cell rearrangements.

(A) Experimentally observed correlations in division patterns between sister (S_1,S_2, n=841) and cousin cells (C_1,C_2, n=580), for cell pairs where neither cell died. **(B)** Correlations in division pattern between cousin cells (C_1,C_2) for simulations of the two-compartment model, for increasing cell rearrangement rate r. Here, the product $r{\cdot}T$, where T is the average cell cycle duration, indicates the approximate number of rearrangements experienced per cell cycle. For a 'well-stirred' proliferative compartment, $r{\cdot}T \gg 1$, asymmetric lineage outcome is more prevalent that symmetric outcome for cousin cells. However, for infrequent cell rearrangements, $r{\cdot}T \approx 1$, asymmetric lineage outcome for cousin cells is less prevalent that symmetric outcome, with a frequency that resembles that seen experimentally in (A). Data is averaged over 50 independent simulations, with $\alpha_p = -\alpha_n = 0.95$, $\phi = 0.95$, and the average number of proliferating cells $\langle D \rangle = 30$. **(C)** Example lineage trees obtained from simulations for different $r{\cdot}T$. Line color indicates whether the cell was in the proliferative (green) or non-proliferative compartment (blue). For $r{\cdot}T = 1$, closely related cells remain largely together in space, causing ejections from the proliferative compartment to be correlated within lineages. As a consequence, not only sisters, but also cousins and more distantly related cells keep proliferating or cease proliferation together. For $r{\cdot}T = 100$, this correlation within lineage trees is lost. **(D)** Coefficient of variation of the total number of proliferating cells D for simulations with a 'well-stirred' proliferative compartment, $r{\cdot}T$ =100. Left panel shows the effects of varying the growth rates of both compartments when all divisions are symmetric and right panel of varying the degree of symmetry when both compartments have opposite growth rates. Overall, the coefficient of variation shows a similar dependence on parameters as seen for the simulations with infrequent cell rearrangements, $r{\cdot}T = 1$, shown in Fig. 4 in the main text.

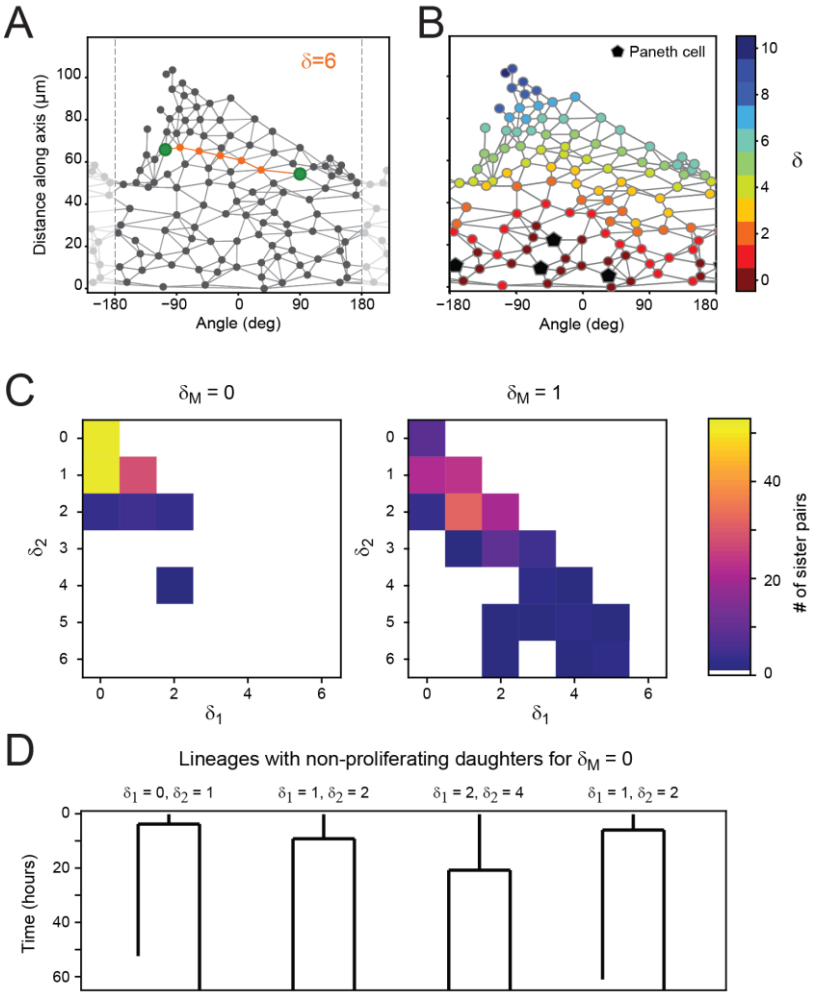

806

807 **Figure S6. Proliferation dynamics as function of Paneth cell distance.**

808 **(A)** After crypt unwrapping and determination of neighbors, the link distance δ between two cells
809 (green markers) is defined as the number of edges that constitute the shortest path connecting the
810 two cells (indicated in orange, resulting in this case in a neighbor distance of δ=6. **(B)** Link distance δ
811 of each cell to its closest Paneth cell, shown for a single time point. **(C)** Distribution of Paneth cell
812 distances δ_1 and δ_2 of sister pairs generate from a mother cell either directly touching a Paneth cell
813 (δ_M=0) or one cell removed from a Paneth cell (δ_M=1). **(D)** Examples of cell lineages for rare sister pairs
814 that ceased proliferation, even though their mother was touching a Paneth cell (δ_M=0). For each sister
815 pair, the distances δ_1 and δ_2 after division are given.